# Surface-Initiated SET Living Radical Polymerisation for the Synthesis of Silica–Polymer Core–Shell Nanoparticles

Jessica Tom,[1] Kohji Ohno,[2] Sébastien Perrier[1,3,4,*]

[1]*Key Centre for Polymers & Colloids, School of Chemistry, The University of Sydney, NSW 2006, Australia.*
[2] *Institute for Chemical Research, Kyoto University, Uji, Kyoto 611-0011, Japan.*
[3] *Department of Chemistry, The University of Warwick, Gibbet Hill, Coventry, CV4 7AL, United Kingdom*
[4] *Faculty of Pharmacy and Pharmaceutical Sciences, Monash University, 381 Royal Parade, Parkville, VIC 3052, Australia*
[*]*email: s.perrier@warwick.ac.uk; Tel: +44 (0)2476 528085; Fax: +44 (0)2476 524112*

## Abstract

We report the use of surface-initiated single-electron transfer living radical polymerisation (SI SET-LRP) to prepare inorganic-organic core–shell nanoparticles with functional grafted chains of high molecular weight. The potential of SI SET-LRP is demonstrated by the preparation of a series of silica–polymer core–shell materials from a silica nanoparticle template bearing a bromo ester initiating group in the presence of a free initiator, with detailed kinetic investigations using methyl acrylate and *tert*-butyl acrylate. Under optimised polymerisation conditions, concentrated polymer brushes with grafting densities as high as 0.8 chains $nm^{-2}$ and relatively high molecular weight polymer grafts (degree of polymerisation, $DP_n$, up to 1000) were achieved whilst employing a heterogeneous copper(0) wire catalyst at low polymerisation temperatures. Under optimal conditions, the polymer shell grows similarly to the free polymer with increasing monomer conversion to produce well-defined monodisperse particles with a narrow size distribution. The particle uniformity results in the formation of particle assemblies that display long-range 2D and 3D order, as characterised by electron microscopy.

## Introduction

Inorganic-organic core–shell nanostructures have gathered significant research interest due to their unique physical and chemical properties.[1] Among them, silica–polymer hybrid materials are the most prominent,[2, 3] owing to their wide range of applications and the ease of synthesis of colloidal silica since the introduction of the Stöber method in 1968.[4] This method affords highly monodisperse particles of a tuneable size ranging from 50 to 2000 nm. Furthermore, the introduction of initiating groups onto the silica surface is easily achieved through the surface hydroxyl moieties, from which dense polymer brushes can be grown.

Core–shell nanostructures are predominantly used as fillers with improved dispersion in polymer composites. However, highly monodisperse inorganic-organic core–shell nanostructures have emerged in a number of interesting and advanced technologies, from drug delivery to colloidal crystals, and in photonics.[5-7] The properties of core–shell structures are strongly influenced by the nature and uniformity of the polymer grafts. For instance, the polymer graft length and grafting density has been shown to impact the circulation lifetime[8] and cytotoxicity[9] of administered nanomaterials, as well as the mechanical properties in polymer composites.[10] Contrary to planar substrates, high grafting densities and ultrahigh molecular weight polymer grafts must be accessible in order to tune the properties of core–shell structures effectively. Indeed, the effective graft density decreases when moving away from a spherical surface, as the chains collapse. As such, increasing the chain length does not significantly affect the shell size. The grafting-from or surface-initiated polymerisation (SIP) approach is preferred, where the polymer chains are grown directly from initiating sites decorating the surface,[11] to form highly dense polymer brushes.

Among the available polymerisation techniques explored, surface-initiated living radical polymerisation (SI-LRP) has proven to be the most powerful, robust, and versatile tool to prepare core–shell materials with precise control over surface functionality due to the wide number of monomers that can be polymerised and copolymerised.[5] With superior control, wide range of polymerisable monomers, and chemical tolerance to impurities, including water and limited oxygen, ATRP is the most widely used LRP technique to prepare particle brushes. SI-ATRP has been successfully applied with a range of common monomers including styrene (S),[12, 13] n-butyl acrylate (nBA),[14, 15] methyl acrylate (MA),[13] methyl methacrylate (MMA),[14, 16-19] and *tert*-butyl acrylate (*t*BA),[13, 20] to more functional monomers such as styrene sulfonate,[19, 21-23] under a range of conditions. However, the large concentration of transition metal required, up to 10,000 ppm, has prompted renewed interest in nitroxide mediated polymerisation (NMP) and reversible–addition fragmentation chain-transfer (RAFT) that proceed in the absence of a catalyst.

Ohno and coworkers[24] reported the synthesis of a novel silane-functionalised RAFT agent that enabled a grafting density as high as 0.8 trithiocarbonate groups $nm^{-2}$ to be achieved. Its similarity to conventional free radical polymerisation (FRP) in combination with its mild polymerisation conditions, number of amenable monomers, chemical tolerance, and ease of chain-end functionalisation, make RAFT more attractive and viable for industrial application. Since this seminal work, which reported the preparation of monodisperse core–shell particles with S, MMA, NIPAAm, and nBA, with grafting densities as high as 0.3 chains $nm^{-2}$, MA, BA, *t*BA, solketal acrylate, AA, 6-(acrylamido)hexanoic acid, MAA, AAm, NIPAAm, DMA, MAAm, S, 4VP, VBC, NAM, MMA, *t*BMA, and 6-azidohexyl methacrylate have been polymerised via SI-RAFT.[2, 24-37] The application of RAFT to prepare core–shell structures has been reviewed recently by Moraes *et al*.[2]

Precise control over these core–shell structures, however, remains hindered by the polymer length that can be synthesised by the SI-LRP techniques in current use due to unavoidable termination. In order to design advanced materials using these core–shell structures with targeted properties, a new tool is needed that is capable of yielding highly dense

and ultrahigh molecular weight polymer grafts, such that the shell size can be accurately controlled by changing the molecular weight targeted.

Currently, the application of single-electron transfer living radical polymerisation (SET-LRP) to functionalise silica nanoparticles has not been reported. SET-LRP offers a unique opportunity to prepare ultrahigh molecular weight polymers with high chain-end retention under ambient conditions.[38-42] SET-LRP also affords products with lower levels of cytotoxic copper salts compared to traditional ATRP techniques in common use due to the heterogeneous catalyst used. The catalyst can be easily removed and recycled, making this technique more viable for industrial use.[38, 39]

In this work, we explore the application of a heterogeneous catalytic system on the SIP of a series of vinyl monomers from initiator-fixed silica nanoparticles (SiP-Br). We also demonstrate the versatility of using SI SET-LRP by exploring other functional monomers including *tert*-butyl acrylate (*t*BA), n-butyl acrylate (nBA), *N*-isopropylacrylamide (NIPAAm), and styrene (S).

## Results and Discussion

Monodisperse silica nanoparticles with an average diameter of 130 nm bearing a bromine-initiating group introduced through a silane coupling agent, {[(2-bromo-2-methylpropionyl)oxy]propyl}triethoxysilane (BPE),[18] were used to study the growth of dense polymer brushes in the presence of a heterogeneous catalytic system. As the SET-LRP of methyl acrylate (MA) is a well-studied and understood system,[40-46] the initiator-fixed silica nanoparticles were used to mediate the growth of poly(methyl acrylate) brushes from the particle surface. All polymerisations were carried out in DMSO at 30 °C using a Cu(0)/$Me_6$TREN catalytic system in the presence of a free (sacrificial) initiator, ethyl 2-bromoisobutyrate (EBiB), unless specified otherwise. Ohno and coworkers[18] have demonstrated the importance of using a free initiator to prepare functionalised nanoparticles. The free polymer formed in solution hinders particle diffusion, preventing interparticle coupling and gelling. It has also been shown that the free initiator facilitates the accumulation of sufficient Cu(II) in SI-ATRP for effective control.[3, 5] The free or unbound polymers formed are easily collected from the supernatant for analysis by $^1H$-NMR and size exclusion chromatography (SEC) to determine the nature of the grafted chains, thus circumventing the need to cleave the bound polymer chains from the surface of the silica particles using HF etching for subsequent analysis. The initiator-fixed particles account for 1 % of the total reaction mixture by weight; this ensures the relative quantity of fixed initiator to free initiator in solution is negligible. As such, the molecular weight of the grafted chains is controlled by the ratio of monomer to free initiator added. All experimental procedures are detailed in the Electronic Supporting Information (ESI).

**Surface-Initiated Polymerisation of Methyl Acrylate from Initiator-Fixed Silica Nanoparticles.** In initial studies, a monomer to initiator ratio of 250 was used. The kinetic results in the absence and presence of initiator-fixed particles are shown graphically in Figure 1. In both cases, the polymerisation proceeded with very similar kinetics, reaching ~80 % conversion within 60 min. In a similar manner to all ATRP-type systems,[47] the polymerisations exhibit poor control within the early stages of the polymerisation. However, as the polymerisation proceeds, the dispersity gradually decreases to ~1.1 in both the free and grafting reaction, until a substantial amount of the Cu(II) deactivator is formed to reversibly capture growing radicals and prevent bimolecular coupling. Despite this, the molecular weight of the free polymer and homopolymer, formed in the absence of functionalised particles, are in agreement with the theoretical molecular weight based on monomer conversion, suggesting that both reactions proceed in a controlled fashion. A slightly decreasing semilogarithmic plot is observed in the presence of functionalised particles. This may be a consequence of the reaction medium being slightly more viscous in the presence of the functionalised particles, which would result in localised heating and consequently a higher occurrence of biomlecular termination associated with higher local radical concentrations. The SIP of MA targeting a *DP* of 500 and 1000 monomer units was also explored under various conditions (Table S1, Entries 2–4). Complete kinetic results are shown in the Electronic Supporting Information (ESI Figure S1 and S2). In a similar manner to the $MA_{250}$ system, the molecular weight distribution is initially broad, but narrows to 1.1–1.2 in both systems at high conversion. The polymerisations all proceed in a living fashion below 80 % conversion regardless of the conditions used, with the semilogarithmic plot increasing linearly with time.

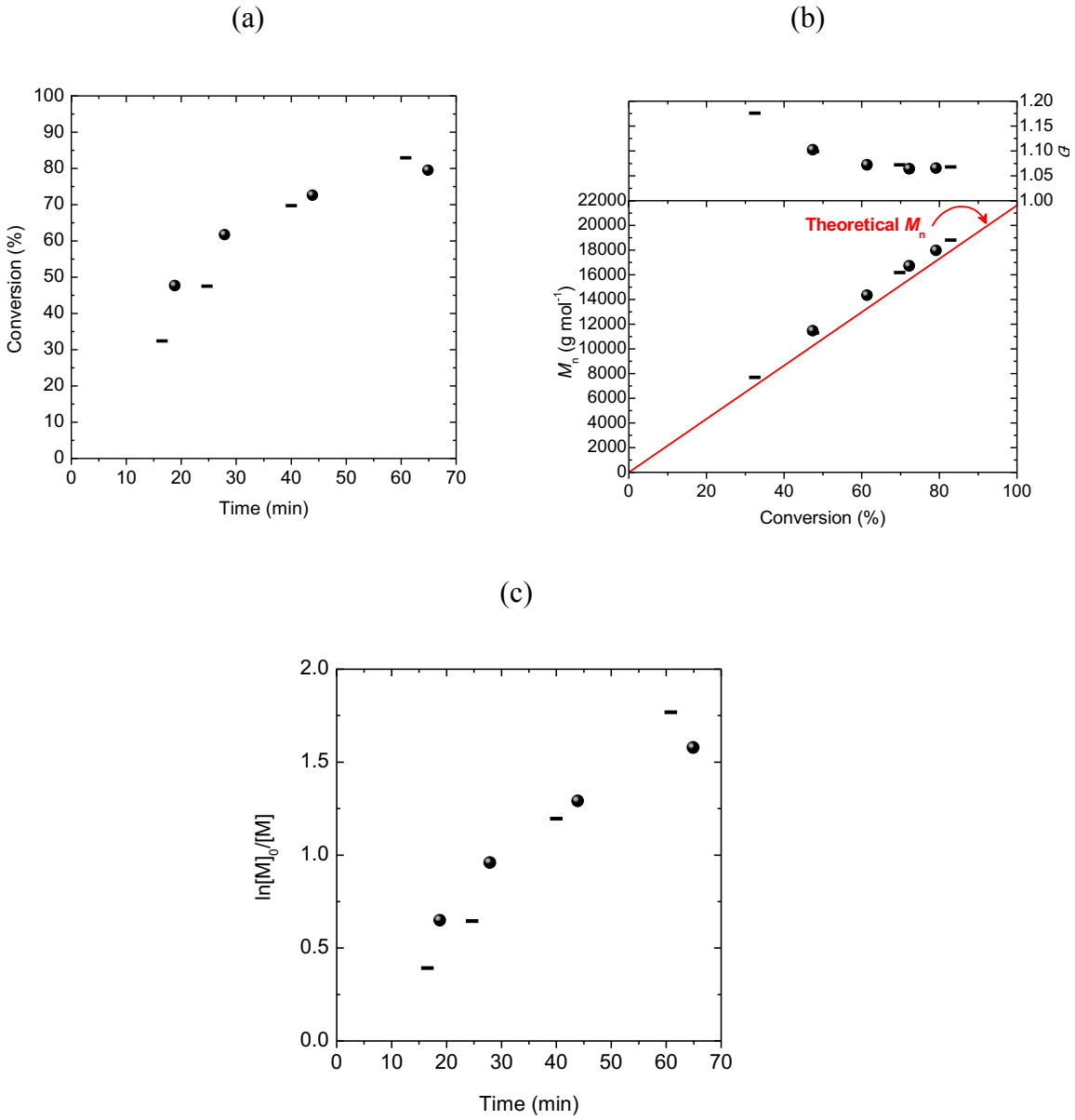


**Figure 1. Kinetic plots monitoring the polymerisation of MA by SET-LRP in DMSO in the absence (–) and presence (•) of 1 % (w/w) SiP-Br. Reaction Conditions: [MA]:[EBiB]:[$Me_6$TREN] = 250:1.00:0.10, MA = 2.0 mL, DMSO = 1.5 mL, 30 °C. Glacial acetic acid activated copper(0) wire (1.5 cm, 1 mm diameter).**

**Polymer Grafting Density.** Thermogravimetric analysis (TGA) confirmed the successful growth of PMA from the surface-bound initiating sites as shown in Figure S4 in the Supporting Information. The bound polymer chains grow in a controlled fashion similar to the free polymer in solution as indicated by the increasing organic content relative to the inorganic silica. The relative quantity of organic to inorganic material was used to calculate the surface grafting density, $\sigma$, according to the ESI Equation (S1). The theoretical molecular weight of the free polymer was used as a representation of the grafted chains. The grafting density over the course of the polymerisation is shown in Figure 2. In all cases, the grafting density increases rapidly to 0.7–0.8 chains nm$^{-2}$. It is expected that the surface-fixed initiators are not activated simultaneously with the free initiator since the initial activation relies on the ability of the particles to approach the copper wire surface. The bound initiators are activated simultaneously

upon the formation and dispersion of the "nascent" Cu(0) nanoparticles throughout the reaction medium,[46] and then continue to grow uniformly since the grafting density is observed to reach a maximum value rapidly. Otherwise, access to the bound initiating sites would be sterically hindered, preventing further activation and growth from other initiating sites decorating the surface.

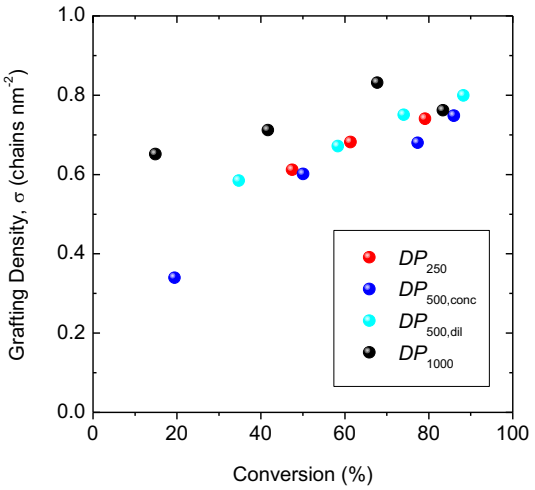


**Figure 2. Evolution of grafting density with increasing monomer conversion whilst targeting a degree of polymerisation of 250 (red markers), 500 under concentrated (blue markers) and dilute (light teal markers) polymerisation conditions, and 1000 (black markers) monomer units.**

**Relative Amount of Organic to Inorganic Material.** The ratio between the organic and inorganic content, denoted $w_g$, can provide an indication of when the bound initiating groups are activated relative to the free initiator with increasing monomer conversion. As shown in Figure 3(a), the SIP is offset relative to the polymerisation of the free initiator, with the surface-fixed initiators not activated until up to ~16 % monomer has been polymerised in the case of $MA_{250}$. As such, the molecular weight of the polymer grafts is expected to be lower than the free polymer. If the delay in the SIP is considered, the grafting densities may actually exceed 0.9 chains nm$^{-2}$. It is important to note here that as the system is diluted, the SIP occurs earlier due to improved diffusion of the particles to the catalyst surface. The SIPs proceed in a controlled manner, with the weight fraction of polymer observed to increase linearly with monomer conversion in all cases. However, in the case of $MA_{500,conc}$, a second stage is observed that is accompanied by a sudden increase in the calculated grafting density. Due to the high density of polymer grafted to the surface at this stage, it is unlikely additional initiating sites are activated due to steric hindrance. Shorter dormant chains may be reinitiated and grow further; rapid polymerisation may occur from the bound chains due to the surface gel or Trommsdorff Effect;[48, 49] or there may be significant free polymer-graft radical coupling occurring, which is supported by the decreasing semilogarithmic plot, particularly at higher conversion in the presence of silica nanoparticles (ESI Figure S1(c)). If we account for the grafting density (Figure 3(b)), it is apparent that the surface groups are activated simultaneously, and grow in a controlled manner similarly to the free polymer in solution. As expected, we also observe that doubling the monomer to free initiator ratio doubles the amount of polymer attached to the surface, and so the graft length is controlled by the amount of monomer to free initiator added.

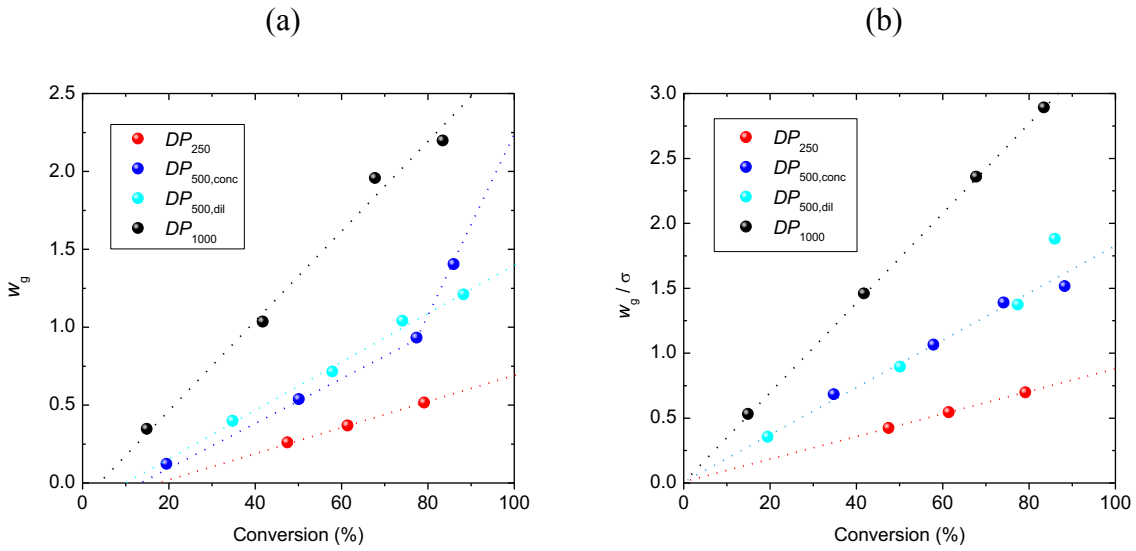


**Figure 3. Weight fraction of PMA to silica with increasing monomer conversion before (a) and after (b) accounting for the polymer grafting density targeting a range of molecular weights under various conditions.**

**Core–Shell Structure and Morphology.** The structure and morphology of the prepared inorganic-organic core–shell particles was examined using electron microscopy. The samples were prepared by dropping a dilute suspension of the SiP-*g*-PMA in $CHCl_3$ onto a TEM grid, and then dried overnight under ambient conditions. The electron micrographs shown in Figure 4 clearly demonstrate the formation of well-defined core–shell structures in all cases. The PMA-*grafted* silica nanoparticles have an even shell thickness and consistent core coverage. The particles further assembled into ordered hexagonal arrays, with no significant aggregation observed. This observation further indicates the prepared core–shell materials are highly uniform and well-defined, and therefore are promising in the formation of colloidal crystals for application in tuneable photonics. The controlled growth of the polymer shell over the course of the polymerisation can be seen in Figure S5 in the ESI, with the polymer shell coating increasing with time. The polymer coating varied from 9 to 37 nm depending on the reaction parameters used. While the rapid increase with time of aggregate sizes observed by dynamic light scattering (DLS) (ESI Figure S3) strongly suggests significant interparticle coupling in the $MA_{500}$ system under both concentrated and dilute conditions, the core–shell particles formed ordered arrays over relatively long length scales, with some shell overlapping observed. Since DLS is biased towards larger species, the contribution of coupled species may be significantly overestimated in this case, further supported by the broadening of the DLS distributions with increasing monomer conversion.

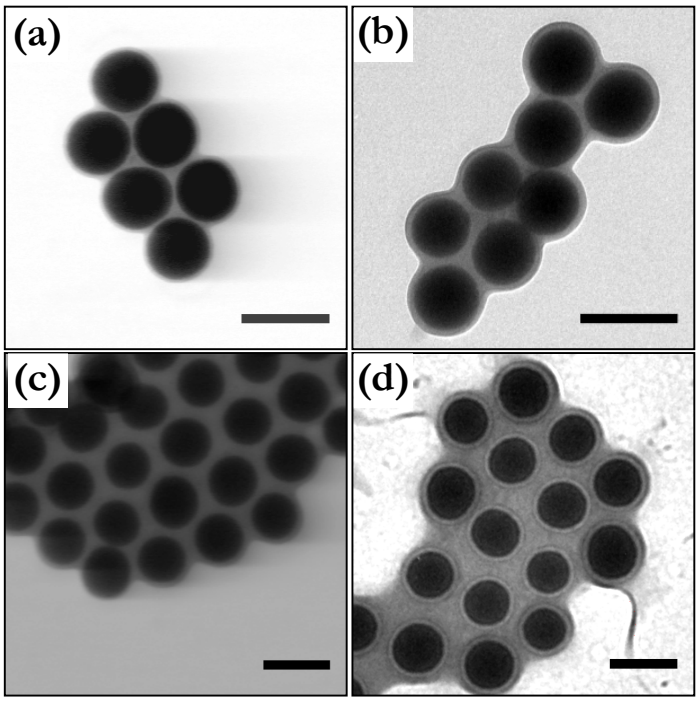


**Figure 4. Electron micrographs of PMA-*grafted* silica nanoparticles (diameter 130 nm) corresponding to free polymer molecular weights of (a) 17200, (b) 37700 (c) 38200, and (d) 71900 g mol$^{-1}$. Scale bar represents 200 nm.**

Ultrahigh molecular weight polymeric brushes were obtained by performing the SIP at 60 °C and targeting a *DP* of 5000 monomer units. The reaction conditions used are summarised in ESI Table S1, Entry 5. The reaction led to the formation of a gel; however, particles could be recovered and these formed highly ordered 2D and 3D arrays with a very thick polymer coating (Figure 5).

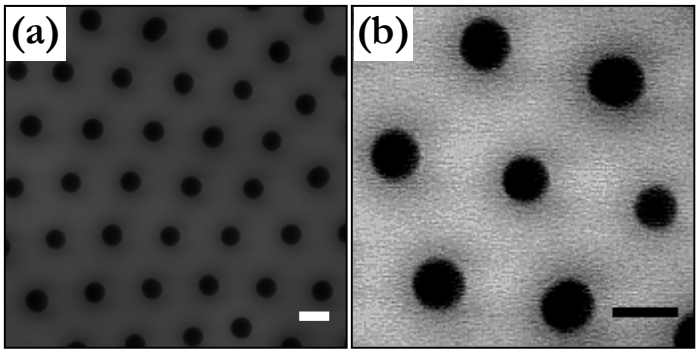


**Figure 5. Scanning transmission electron micrographs of PMA-*grafted* silica nanoparticles (diameter 130 nm) targeting a $DP_n$ of 5000 monomer units polymerised at 60 °C at various magnifications. Scale bars represent 200 nm.**

Since SET-LRP offers near perfect chain end functionality retention, we attempted to perform successive chain extensions to build up the shell thickness. This approach is depicted in ESI Scheme S2, and the experimental conditions and procedure followed are detailed in the ESI. As observed in the electron micrographs (Figure 6(a) and 6(b)), after the initial SIP targeting a *DP* of 1000 monomer units, the prepared core–shell particles are well-defined and pack into highly ordered hexagonal arrays. However, this long-range order is destroyed after chain extension ((Figure 6(c) and 6(d)). While the first block appeared to proceed in a living fashion with a sustained pale yellow solution observed, the solution quickly developed an

intense green colour when performing the block extension, only reaching 24 % conversion after 4 h compared to 51 % after 130 min for the first block.

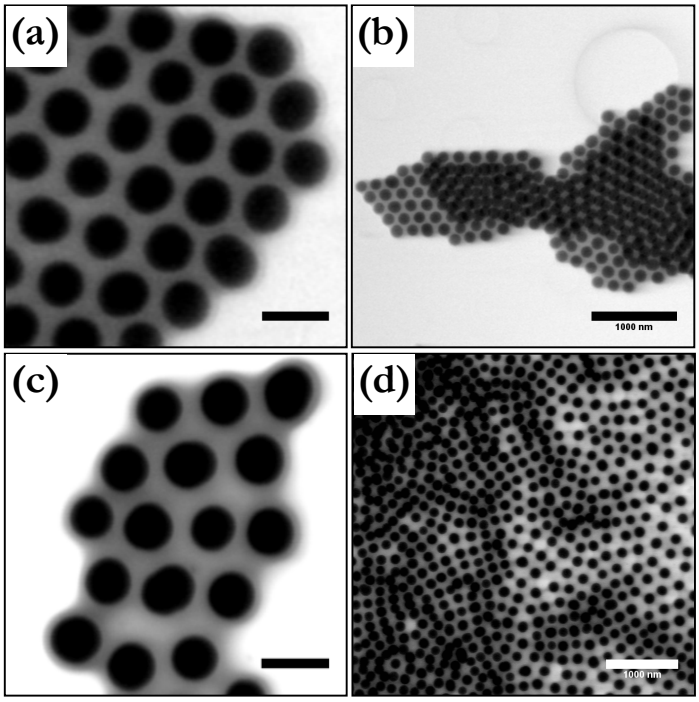


**Figure 6. (a)–(b) Scanning transmission electron micrographs showing the structure and uniformity of PMA-*grafted* silica nanoparticles, SiP-*g*-PMA, in comparison to the (c)–(d) chain-extended SiP-*g*-(PMA-*b*-PMA). Scale bars represent 200 nm, unless specified otherwise.**

**Exploring the Versatility of SET-LRP to Prepare Silica–Polymer Hybrid Materials.** Having shown the efficacy of SI SET-LRP to prepare core–shell materials using MA, we further explored its application using a series of monomers with varying physical properties. Detailed kinetic investigations were carried out to investigate the growth of poly(*tert*-butyl acrylate) brushes over a range of molecular weights, and comprehensive results are shown in the ESI, Figure S6 to S12. The polymerisations were carried out in trifluoroethanol (TFE) in accordance to recent reports by Percec and coworkers.[50-52] After initial studies at 30 °C (ESI Figure S6), a higher temperature of 50 °C was chosen for the SIP of *t*BA to achieve higher monomer conversions. The results are summarised in Table 1.

All SIPs of *t*BA exhibited poor control within the early stages with very broad dispersities. However, the molecular weight distribution decreased rapidly to 1.1 at high conversion in all cases in a similar manner to the MA system. The broader molecular weight distributions observed initially can be attributed to the poorer disproportion of Cu(I) generated *in situ* in TFE due to the formation of a less stable Cu(II) complex compared with DMSO and other dipolar aprotic solvents.[50] The SIP of *t*BA also proceeds in 2 distinct stages. First, there is a rapid polymerisation due to an insufficient quantity of the Cu(II) deactivating species. This is followed by a slower polymerisation once the SET-LRP equilibrium has been established and further polymerisation is impeded by the high viscosity medium. The rate within the second stage is generally higher in the presence of silica nanoparticles (SiNPs), attributed to localised heating. The P*t*BA grows from the surface in a controlled fashion in all cases, with the hydrodynamic diameter ($D_h$) of the core–shell particles increasing with increasing monomer conversion (ESI Figure S10). In the $t\text{BA}_{250}$(50 °C) system, the growth of the surface-bound polymer appears to plateau between 60 and 100 min, followed by renewed growth, accompanied by a noticeable increase in viscosity. This behaviour results from the Trommsdorff Effect. The preparation of well-defined core–shell structures was confirmed by

electron microscopy (Figure 7), with an average shell thickness increasing with monomer conversion (ESI Figure S12) in agreement with those calculated for a collapsed polymer shell. There is also clear evidence of interparticle coupling in the *t*BA$_{370}$ system (ESI Figure S12). In this system, the Trommsdorff Effect was clearly observed for both particle and free polymerisation systems (ESI Figure S8). In addition, the SiP-*g*-P*t*BA core–shell materials formed less ordered arrays than the MA system. Despite this, the core–shell particles appeared well-defined, achieving a shell thickness up to (39.4 ± 6.1) nm.

**Table 1 Summary of the silica–polymer core–shell materials formed by SIP, characterised using $^1H$-NMR, SEC, TGA, and electron microscopy, in comparison to the modelled theoretical size.**

| | | | | | | $^1H$-NMR[a] (Free Polymer) | | | SEC[b] (Free Polymer) | | | TGA[c] | Core–Shell Models[d] | | Electron Microscopy[e] |
|---|---|---|---|---|---|---|---|---|---|---|---|---|---|---|---|
| | *Monomer* | $DP_{n,target}$ | *T* (°C) | *M*:*S* (v/v) | *t* (min) | %C | $DP_{n,th}$ | $M_{n,th}$ | $M_{n,SEC}$ | $M_{w,SEC}$ | *Đ* | $\sigma$ (chains nm$^{-2}$) | $\overline{D}_{cc}$ (nm) | $\overline{D}_{ext}$ (nm) | $\overline{D}$ (nm) |
| 1 | MA | 250 | 30 | 2:1.5 | 65 | 79.3 | 197 | 17200 | 17900 | 19100 | 1.06 | 0.74 | 158 | 229 | 149 ± 3 |
| 2 | | 500 | 30 | 2:1 | 81 | 86.1 | 435 | 37700 | 41400 | 46100 | 1.11 | 0.75 | 187 | 349 | 159 ± 8 |
| 3 | | | 30 | 2:1.5 | 62.4 | 88.4 | 441 | 38200 | 37400 | 40200 | 1.07 | 0.80 | 186 | 352 | 171 ± 7 |
| 4 | | 1000 | 30 | 1:1 | 120 | 83.6 | 833 | 71900 | 83300 | 91400 | 1.10 | 0.76 | 214 | 549 | 203 ± 13 |
| *5* | | 5000 | 60 | 1:1 | 810 | 64.0 | 3200 | 275600 | - | - | - | 1.15 | 359 | 1740 | 394 ± 29 |
| *6* | *t*BA | 250 | 30 | 2:1 | 360 | 27.2 | 69 | 8840 | 8100 | 8600 | 1.06 | 0.35 | 139 | 165 | 151 ± 5 |
| 7 | | | 50 | 2:1 | 148 | 62.5 | 157 | 20290 | 21300 | 22300 | 1.04 | 0.43 | 153 | 209 | 155 ± 3 |
| 8 | | 370 | 50 | 2:1 | 162 | 85.1 | 317 | 40780 | 40700 | 43300 | 1.06 | - | - | 290 | 150 ± 8 |
| 9 | | 745 | 50 | 2:1 | 245 | 74.1 | 551 | 70850 | 82300 | 89700 | 1.09 | 0.59 | 207 | 407 | 209 ± 12 |
| 10 | nBA | 250 | 30 | 2:1.5 | 1440 | 49 | 123 | 16000 | 20600 | 21800 | 1.06 | 0.33 | 145 | 192 | 141 ± 5 |
| 11 | NIPAAm | 260 | 30 | 2:3* | 1440 | 20 | 52 | 6100 | 39000 | 110700 | 2.80 | 0.25–0.94 | 146 | 156 | 145 ± 4 |
| 12 | S | 250 | 90 | 2:1 | 1440 | 67 | 169 | 17800 | 19100 | 20900 | 1.10 | 0.09 | 135 | 215 | 143 ± 4 |
| 13 | AA | - | - | - | - | - | 157 | 11500* | - | - | - | 0.61 | 149 | 209 | 155 ± 10 |

[a]The monomer conversion was determined by $^1H$ NMR. $DP_{n,th}$ = ([Monomer]$_0$/[EBiB]$_0$ × conversion). $M_{n,th}$ = ($DP_{n,th}$ × $MW_{Monomer}$) + $MW_{EBiB}$

[b]$M_{n,SEC}$, $M_{w,SEC}$ and *Đ* were determined by size exclusion chromatography against PS standards.

[c]Determined by thermolysis (700 °C, $O_2$ atm). Equation (S1) was used to calculate the grafting density, $\sigma$, accounting for the residual organic matter present on the surface of the silica nanoparticles.

[d]$\overline{D}_{cc}$ and $\overline{D}_{ext}$ correspond to the compact core–shell and extended core–shell particle diameters.

[e]The average centre-to-centre distance, $\overline{D}$, was determined by electron microscopy.

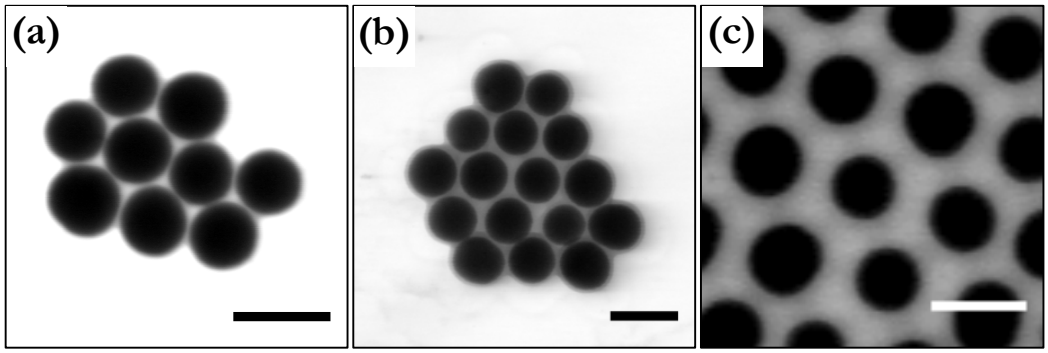


**Figure 7. Electron micrographs of P*t*BA-*grafted* silica nanoparticles (diameter 130 nm) corresponding to free polymer molecular weights of (a) 20286, (b) 39693, and (c) 70800 g mol$^{-1}$. Scale bar represents 200 nm.**

The final grafting density achieved for P*t*BA (Table 1, ESI Figure S11) ranged between 0.35 and 0.59 chains $nm^{-2}$, which is significantly lower than those obtained for MA (0.7–0.8 chains $nm^{-2}$). The initial Cu(II) deficit contributes to a high incidence of termination, as well as the rapid polymerisation of the active sites. This provides a steric barrier for further activation of the bound initiating groups, resulting in the lower apparent grafting density observed in these systems. A higher grafting density of 0.75 chains $nm^{-2}$ was achieved for the $tBA_{370}$ system at a monomer conversion of 90.9 %, which is comparable to those achieved for MA. The higher grafting density is a consequence of the very rapid polymerisation of the free initiator. The highly viscous medium hindered the diffusion of the functionalised particles to the catalyst surface, which delayed the SIP until the nascent Cu(0) nanoparticles were dispersed throughout the system.

The SIP of n-butyl acrylate (nBA), *N*,*N*-isopropylacrylamide (NIPAAm) and styrene (S) were also attempted using a monomer to free initiator ratio of ~250. In addition to this, we showed that carboxylate functions could be accessed by the deprotection of P*t*BA-*coated* silica nanoparticles by acid hydrolysis. In all cases, the polymerisation was quenched after 24 h and the polymer-*coated* silica nanoparticles collected and washed for characterisation. Our preliminary results are summarised in Table 1, and the core–shell structures are shown in Figure 8. Detailed experimental procedures are provided in the ESI, with the reaction conditions and stoichiometric quantities used are summarised in Table S1, Entries 10–12.

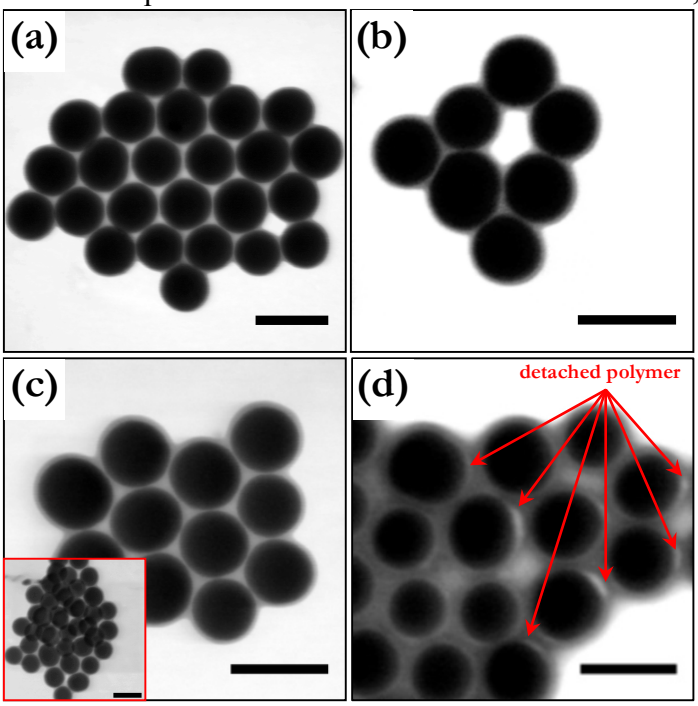


**Figure 8. Electron micrographs of silica nanoparticles coated with (a) PnBA, (b) PNIPAAm, (c) PS, and (d) PAA. Inset shows agglomerated core–shell nanoparticles. Scale bar represents 200 nm.**

PnBA brushes, thoroughly explored on a diverse range of substrates for their elastomeric properties,[15, 53] resulted in the formation of highly ordered arrays (Figure 8(a)). This behaviour indicates the core–shell structure formed is well-defined. However, under the prescribed conditions, a limited monomer conversion of 49 % was achieved after 24 h as a consequence of accumulated Cu(II), indicated by the development of an intense green colour. The disproportionation of the Cu(I)Br/$Me_6$TREN complex formed *in situ* is expected to be significantly slower in nBA, being more hydrophobic than MA. This results in a large local influx of radicals at the copper(0) wire surface leading to significant bimolecular termination and the accumulation of Cu(II)$Br_2$.

Exploiting a responsive polymer such as PNIPAAm, with its characteristic volume phase transition at ~32 °C, has great potential in the generation of so-called "smart" materials for controlled drug delivery to separation applications. The SIP was performed using a copper(0) wire/PMDETA catalytic system. While the polymerisation from the free initiator was poorly controlled with a dispersity of 2.8 at 20 % monomer conversion, the core–shell structure appeared to be uniform, with the polymer clearly encasing the silica core as shown in Figure 8(b), and a corresponding *PDI* of 0.03 by DLS. The PNIPAAm chains retained their sensitivity to thermal stimuli despite being tethered to a solid support as shown in Figure 9. The surface curvature and low grafting density in this case is advantageous, allowing the chains to move more freely as they interact less with neighbouring chains. The volume phase transition remained unchanged from the free polymer of approximately 32 °C.

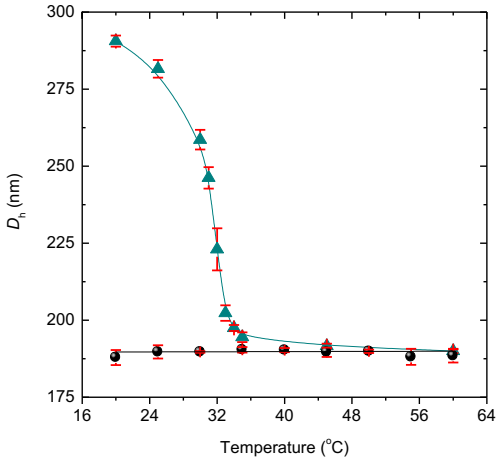


**Figure 9. Hydrodynamic diameter with increasing temperature of PNIPAAm-*grafted* silica nanoparticles (▲) in comparison to initiator-fixed silica nanoparticles (●).**

Attempts to grow PS brushes at 90 °C using a modified literature procedure[54] yielded core–shell particles that exhibited short-range order (Figure 8(c)) with significant evidence of aggregation (Inset, Figure 8(c)). The low grafting density of 0.09 chains $nm^{-2}$ was further supported by electron microscopy, where the polymer shell is clearly compressed between particles. The low grafting density arising from the permanent loss of chain ends at the beginning of the polymerisation is in agreement with the significant Cu(II) accumulated, as indicated by the observed intense green colour of the solution.[55] While nonpolar solvents have been shown to mediate the disproportionation of Cu(I)Br in the presence of $Me_6$TREN,[55] the poor solubility of the $CuBr_2$/$Me_6$TREN complex resulted in poor chain-end fidelity, and as such, our findings are not surprising. Despite this, the free polymerisation proceeded to a high conversion (67.3 %) after 24 h, and the core–shell particles were easily purified by the addition of an aqueous solution of EDTA during the washing cycle.

Acidic polymers are compatible with biological and aqueous environments, they are suitable candidates to prepare "smart" materials, responding to pH changes, and are easily conjugated to biologically active molecules such as drugs or dyes through carbodiimide coupling. However, monomers bearing acidic moieties are generally not compatible with metal-mediated polymerisations.[56] Consequently, to end, we wanted to show that acidic polymers could be accessed since they are of great interest in a variety of fields including drug delivery, controlled-release coatings, biomolecule immobilisation, sensors and membrane transport.[56] Acrylic acid-*coated* silica nanoparticles were achieved by a sequential polymerisation-deprotection approach. *Tert*-butyl acrylate was first polymerised from initiator-fixed silica ($DP_{n,target}$ 250), and the *tert*-butyl ester groups were then hydrolysed using

trifluoroacetic acid (TFA) for 24 h. The removal of the *tert*-butyl groups was confirmed by FT-IR (ESI Figure S13(a)) and TGA (ESI Figure S13(b)). The resultant material was easily dispersed in alcohols and water, and no longer dispersible in organic solvents such as DCM. While the particles appear uniform by DLS with a very narrow *PDI* of 0.095, voids are clearly visible between the silica surface and the polymer shell in the electron micrograph (Figure 8(d)) where the polymer has detached from the surface, in addition to significant agglomeration observed. The ester function linking the initiator to the surface proved vulnerable to acid hydrolysis. This result was unexpected with the precipitation of the hydrolysed material once a significant portion of the pendant groups had been hydrolysed. This may arise due to the curvature of the surface and low polymer grafting density. Despite this, the prepared particles became increasingly negative with increasing pH with the deprotonation of the attached carboxylic acid pendant groups (Figure 10).

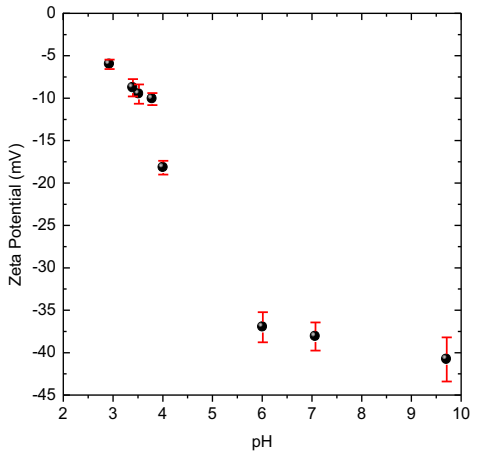


**Figure 10. Zeta potential of PAA-*coated* silica nanoparticles with increasing pH.**

## Conclusions

In conclusion, we have shown that SET-LRP can be used to generate concentrated polymer brushes grown from spherical monodisperse silica nanoparticles with a diameter of 130 nm. SI SET-LRP proved to be a facile approach to prepare well-defined core–shell structures rapidly in the presence of a free initiator. It was shown that the presence of a sacrificial initiator under optimal conditions controls the molecular weight of the grafted polymer, and hinders particle diffusion to limit interparticle coupling and support the simultaneous activation of the surface-bound initiators to achieve uniform growth and high grafting densities. Relatively high molecular weight polymer grafts ($DP_n \leq 1000$), and grafting densities as high as 0.8 chains $nm^{-2}$ were achieved. The versatility of this approach was further demonstrated by the preparation and characterisation of a series of silica–polymer core–shell materials with MA, *t*BA, nBA, NIPAAm, and styrene. Acidic functionalities were also accessed by the deprotection of P*t*BA-*grafted* silica. The heterogeneous catalyst resulted in low levels of copper contaminants, facilitating easy removal and less arduous material purification. In addition, a number of suitable siloxanes for initiation are commercially available to introduce an initiating group for SI-ATRP or SET-LRP. The application of SI SET-LRP is a step towards core–shell materials with precisely tuneable properties.

## Supporting Information

Detailed core–shell syntheses and reaction conditions used. Characterisation methods and instrument set-up. Polymerisation kinetics using SEC and $^1H$-NMR characterisation. Electron micrographs, DLS, and TGA of the prepared core–shell structures. Calculation of the surface grafting density and mathematical models used to predict the expected and maximum possible shell size.

## Acknowledgements

Dr. John Moraes is acknowledged for the preparation of the SiP-Br particles in collaboration with A/Prof. Kohji Ohno (Institute for Chemical Research, Kyoto University). The authors acknowledge the facilities and technical assistance of the Australian Centre for Microscopy & Microanalysis at the University of Sydney. JT acknowledges the Australian Government for the provision of an Australian Postgraduate Award research scholarship. The Royal Society Wolfson Merit Award (WM130055; SP) and the Monash-Warwick Alliance (SP) are acknowledged for financial support.

## References

1. R. Ghosh Chaudhuri and S. Paria, *Chem. Rev.*, 2012, 112, 2373-2433.
2. J. Moraes, K. Ohno, T. Maschmeyer and S. Perrier, *Chem. Commun.*, 2013, 49, 9077-9088.
3. B. Radhakrishnan, R. Ranjan and W. J. Brittain, *Soft Matter*, 2006, 2, 386-396.
4. W. Stöber, A. Fink and E. Bohn, *J. Colloid Interface Sci.*, 1968, 26, 62-69.
5. J. Pyun and K. Matyjaszewski, *Chem. Mater.*, 2001, 13, 3436-3448.
6. C. M. Hui, J. Pietrasik, M. Schmitt, C. Mahoney, J. Choi, M. R. Bockstaller and K. Matyjaszewski, *Chem. Mater.*, 2014, 26, 745-762.
7. V. Biju, *Chem. Soc. Rev.*, 2014, 43, 744-764.
8. K. Ohno, T. Akashi, Y. Tsujii, M. Yamamoto and Y. Tabata, *Biomacromolecules*, 2012, 13, 927-936.
9. I. C. Lin, M. Liang, T.-Y. Liu, Z. Jia, M. J. Monteiro and I. Toth, *Biorg. Med. Chem.*, 2012, 20, 6862-6869.
10. P. Akcora, H. Liu, S. K. Kumar, J. Moll, Y. Li, B. C. Benicewicz, L. S. Schadler, D. Acehan, A. Z. Panagiotopoulos, V. Pryamitsyn, V. Ganesan, J. Ilavsky, P. Thiyagarajan, R. H. Colby and J. F. Douglas, *Nat. Mater.*, 2009, 8, 354-U121.
11. S. Edmondson, V. L. Osborne and W. T. S. Huck, *Chem. Soc. Rev.*, 2004, 33, 14-22.
12. I. Mora-Barrantes, J. L. Valentin, A. Rodriguez, I. Quijada-Garrido and R. Paris, *J. Mater. Chem.*, 2012, 22, 1403-1410.
13. B. Radhakrishnan, A. N. Constable and W. J. Brittain, *Macromol. Rapid Commun.*, 2008, 29, 1828-1833.
14. J. Pyun, S. Jia, T. Kowalewski, G. D. Patterson and K. Matyjaszewski, *Macromolecules*, 2003, 36, 5094-5104.
15. G. Carrot, S. Diamanti, M. Manuszak, B. Charleux and I. P. Vairon, *J. Polym. Sci., Part A: Polym. Chem.*, 2001, 39, 4294-4301.
16. Y. P. Wang, X. W. Pei, X. Y. He and K. Yuan, *Eur. Polym. J.*, 2005, 41, 1326-1332.
17. K. Ohno, T. Morinaga, K. Koh, Y. Tsujii and T. Fukuda, *Macromolecules*, 2005, 38, 2137-2142.
18. K. Ohno, T. Akashi, Y. Huang and Y. Tsujii, *Macromolecules*, 2010, 43, 8805-8812.
19. K. Ohno, H. Tabata and Y. Tsujii, *Colloid. Polym. Sci.*, 2013, 291, 127-135.
20. N. D. Treat, N. Ayres, S. G. Boyes and W. J. Brittain, *Macromolecules*, 2006, 39, 26-29.
21. B. T. Cheesman, J. D. Willott, G. B. Webber, S. Edmondson and E. J. Wanless, *ACS Macro Lett.*, 2012, 1, 1161-1165.
22. H. Suzuki, M. Murou, H. Kitano, K. Ohno and Y. Saruwatari, *Colloids Surf., B*, 2011, 84, 111-116.
23. E. Labalme, G. David, P. Buvat, J. Bigarre and T. Boucheteau, *J. Polym. Sci., Part A: Polym. Chem.*, 2012, 50, 1308-1316.
24. K. Ohno, Y. Ma, Y. Huang, C. Mori, Y. Yahata, Y. Tsujii, T. Maschmeyer, J. Moraes and S. Perrier, *Macromolecules*, 2011, 44, 8944-8953.
25. R. Ranjan and W. J. Brittain, *Macromol. Rapid Commun.*, 2007, 28, 2084-2089.
26. J. Moraes, K. Ohno, T. Maschmeyer and S. Perrier, *Chem. Mater.*, 2013, 25, 3522-3527.
27. Y. Yang, Z. Yang, Q. Zhao, X. Cheng, S. C. Tiong, R. K. Y. Li, X. Wan and X. Xie, *J. Polym. Sci., Part A: Polym. Chem.*, 2009, 47, 467-484.
28. Y. Huang, Q. Liu, X. Zhou, S. Perrier and Y. Zhao, *Macromolecules*, 2009, 42, 5509-5517.
29. Y. Li and B. C. Benicewicz, *Macromolecules*, 2008, 41, 7986-7992.
30. Y. Zhao and S. Perrier, *Macromolecules*, 2007, 40, 9116-9124.

31. **Y. Zhao and S. Perrier, *Macromolecules*, 2006, 39, 8603-8608.**
32. **C.-H. Liu and C.-Y. Pan, *Polymer*, 2007, 48, 3679-3685.**
33. **C. Z. Li and B. C. Benicewicz, *Macromolecules*, 2005, 38, 5929-5936.**
34. **C. Li, J. Han, C. Y. Ryu and B. C. Benicewicz, *Macromolecules*, 2006, 39, 3175-3183.**
35. **C.-Y. Hong, X. Li and C.-Y. Pan, *Eur. Polym. J.*, 2007, 43, 4114-4122.**
36. **J. Moraes, K. Ohno, G. Gody, T. Maschmeyer and S. Perrier, *Beilstein J. Org. Chem.*, 2013, 9, 1226-1234.**
37. **Y. Guo, H. Liu, D. Tang, C. Li and Y. Zhao, *Polym. Chem.*, 2015, 6, 2647-2658.**
38. **A. Anastasaki, V. Nikolaou and D. M. Haddleton, *Polym. Chem.*, 2016, 7, 1002-1026.**
39. **A. Anastasaki, V. Nikolaou, G. Nurumbetov, P. Wilson, K. Kempe, J. F. Quinn, T. P. Davis, M. R. Whittaker and D. M. Haddleton, *Chem. Rev.*, 2016, 116, 835-877.**
40. **V. Percec, T. Guliashvili, J. S. Ladislaw, A. Wistrand, A. Stjerndahl, M. J. Sienkowska, M. J. Monteiro and S. Sahoo, *J. Am. Chem. Soc.*, 2006, 128, 14156-14165.**
41. **G. Lligadas, B. M. Rosen, M. J. Monteiro and V. Percec, *Macromolecules*, 2008, 41, 8360-8364.**
42. **N. H. Nguyen, M. E. Levere and V. Percec, *J. Polym. Sci., Part A: Polym. Chem.*, 2012, 50, 860-873.**
43. **N. H. Nguyen and V. Percec, *J. Polym. Sci., Part A: Polym. Chem.*, 2010, 48, 5109-5119.**
44. **N. H. Nguyen, B. M. Rosen, G. Lligadas and V. Percec, *Macromolecules*, 2009, 42, 2379-2386.**
45. **M. E. Levere, N. H. Nguyen and V. Percec, *Macromolecules*, 2012, 45, 8267-8274.**
46. **M. E. Levere, N. H. Nguyen, H. J. Sun and V. Percec, *Polym. Chem.*, 2013, 4, 686-694.**
47. **K. Matyjaszewski and J. Xia, *Chem. Rev.*, 2001, 101, 2921-2990.**
48. **J. D. Jeyaprakash, S. Samuel, R. Dhamodharan and J. Rühe, *Macromol. Rapid Commun.*, 2002, 23, 277-281.**
49. **K. Matyjaszewski, P. J. Miller, N. Shukla, B. Immaraporn, A. Gelman, B. B. Luokala, T. M. Siclovan, G. Kickelbick, T. Vallant, H. Hoffmann and T. Pakula, *Macromolecules*, 1999, 32, 8716-8724.**
50. **S. R. Samanta, A. Anastasaki, C. Waldron, D. M. Haddleton and V. Percec, *Polym. Chem.*, 2013, 4, 5555-5562.**
51. **X. F. Leng, N. H. Nguyen, B. van Beusekom, D. A. Wilson and V. Percec, *Polym. Chem.*, 2013, 4, 2995-3004.**
52. **S. R. Samanta, M. E. Levere and V. Percec, *Polym. Chem.*, 2013, 4, 3212-3224.**
53. **J. Parvole, J. P. Montfort, G. Reiter, O. Borisov and L. Billon, *Polymer*, 2006, 47, 972-981.**
54. **J. Tom, B. Hornby, A. West, S. Harrisson and S. Perrier, *Polym. Chem.*, 2010, 1, 420-422.**
55. **M. E. Levere, N. H. Nguyen, X. Leng and V. Percec, *Polym. Chem.*, 2013, 4, 1635-1647.**
56. **B. M. Cash, L. Wang and B. C. Benicewicz, *J. Polym. Sci., Part A: Polym. Chem.*, 2012, 50, 2533-2540.**

## Graphical Abstract